Journal of Physics D: Applied Physics

Simplified human thermoregulatory model for designing wearable thermoelectric devices

Simplified human thermoregulatory model for designing wearable thermoelectric devices

Dimuthu Wijethunge[1], *Donggyu Kim*[1], *and Woochul Kim*[*]

[1]The following authors contributed equally to the presented work

School of Mechanical Engineering, Yonsei University, Seoul 120-749, Republic of Korea

Abstract:

Research on wearable and implantable devices have become popular with the strong need in market. A precise understanding of the thermal properties of human skin, which are not constant values but vary depending on ambient condition, is required for the development of such devices. In this paper, we present simplified human thermoregulatory model for accurately estimating the thermal properties of the skin without applying rigorous calculations. The proposed model considers a variable blood flow rate through the skin, evaporation functions, and a variable convection heat transfer from the skin surface. In addition, wearable thermoelectric generation (TEG) and refrigeration (TER) devices were simulated. We found that deviations of 10–60% can be resulted in estimating TEG performance without considering human thermoregulatory model owing to the fact that thermal resistance of human skin is adapted to ambient condition. Simplicity of the modeling procedure presented in this work could be beneficial for optimizing and predicting the performance of any applications that are directly coupled with skin thermal properties.

Keywords: Skin thermal resistance, Wearable thermoelectric devices, Body heat flux, Thermoelectric generation, Thermoelectric refrigeration , Energy harvesting

[*] Email: woochul@yonsei.ac.kr

1. Introduction

Wearable devices have become increasingly popular in the modern world[1], but owing to their limited battery time, the use of such devices can be an inconvenient and unsatisfactory experience for many users. Under such circumstances, human energy scavenging devices play an import role in making wearable devices self-powered or in increasing the battery time. Efficient thermoelectric materials have recently been developed [2, 3] enabling thermoelectric devices to be used in a wide range of applications. With the improvement of materials, thermoelectric harvesters could be a common feature in many wearable devices in near future. The performance of wearable thermoelectric harvesters is correlated with the thermal properties of the human skin and body. The human body is not an ideal source of energy, and it has a low thermal conductivity; the harvestable energy from the human body is relatively low. Therefore, optimization is essential for scavenging every possible amount of energy while limiting the use of expensive thermoelectric materials. The optimization can be achieved in terms of the thermoelectric element geometry [4, 5], percentage of the filler material[6], and use of a heat sink[7]. A proper thermal model of human skin is a requisite for an accurate prediction of the results.

Considering various studies related to wearable thermoelectric devices, many researchers have overlooked the importance of the human thermoregulatory system, and have treated human skin as an object with a constant temperature or thermal resistance[7-9]. Actually, the human skin is a much more complicated heat source because its properties vary along with many different parameters, such as the ambient conditions and level of physical activity. As an example of wearable thermoelectrics, Leonov *et al.*[10] measured the thermal resistance of human skin experimentally using a thermoelectric generator (TEG) attached to various locations of the human body. In this work, the thermal resistance was calculated by calculating the heat flow through the TEG using measurements of the output voltage of the device. With this method, the authors obtained a thermal resistance of 0.006 to 2 m^2 K/W under different conditions. Bahk *et al.*[8] used Leonav's data to approximate the thermal resistance of the skin in an optimization of a wearable energy harvesting device. The authors used a thermal resistance of 0.02 m^2 K/W for the calculations. Webb *et al.*[11] measured the skin temperatures of different body locations under different conditions, which were used by Suarez *et al.*[9] to calculate the thermal resistance of the skin for predicting the performance of a wearable thermoelectric generator. According to Suarez *et al.*[9], the thermal resistance of the skin is around 0.06667 m^2 K/W. Pietrzyk *et al.*[7] predicted 0.01351 m^2 K/W as the thermal resistance of the skin in their calculations of wearable thermoelectric energy harvesting. Considering recently published studies on wearable thermoelectric devices, non-unified values have been used for the thermal resistance of the skin. Therefore, accurate modeling on this resistance is required to investigate precise values.

Insight for thermal resistance modeling of the skin can be found in studies related to the human thermoregulatory system, which are described below. Few heat transfer models were proposed in the early 19^{th} century. Among them, Pennes's work in 1948 [12] can be considered as the most significant work in the field of bio-heat transfer. Pennes proposed a simple and yet effective equation for a heat transfer in human tissue, which is known as the Pennes bioheat equation. After Pennes, Chen et al.[13] and Jiji et al.[14], developed equations based on the vasculature. These equations were more developed bioheat transfer equations, yet contained excessive parameters. Wissler *et al.*[15] matched their experimental data with Pennes's theoretical data on a resting forearm, and demonstrated that the Pennes bioheat equation has an acceptable level of accuracy. Stolwijk and Hardy [16] developed a well-known multi-node thermoregulatory model called the Stolwijk model. In this model, the body is divided into five cylindrical segments representing the trunk, arms, hands, legs, and head. Each part is then divided into the core, muscle, fat, and skin. The model also uses a variable blood flow rate, shivering and sweating functions. The Stolwijk model also considers parameters such as the height, weight, and fat percentage. Thus, physiological data presented through the Stolwijk model have been widely used to construct other human models. The Smith model [17] is another human multi-element model with three-dimensional transient calculations, and has accurate sudomotor, *i.e.*, evaporation, functions. The sudomotor functions in the Smith model is widely being used to model evaporation. The Fu model [18] is an improvement over the Smith model by introducing a clothing layer. The Fiala model [19] is another popular human thermoregulatory model, which consists of 15 body elements. Each body element is divided into anterior, posterior, and inferior parts. The Fiala model also integrated the thermal sensation into this model. The Berkeley model [20], which is another multi-segment human model, was developed by improving the Stolwijk model. The Berkeley model used an improved blood flow model with a counter current heat exchange. The Foda and Siran model [21] presents an improved calculation on the convective heat transfer.

In this study, we simplified existing human thermoregulatory models so that the model we proposed can be used to design wearable thermoelectric devices or predict skin thermal properties, which are not constant values but vary depending on the ambient condition. Many of the previous models are heavily equipped with numerous functions for accurately simulating the human thermoregulatory system. The complexity of these models prevents them from being used in many applications, such as wearable thermoelectric devices. The main objective in this case is to simulate the device performance, rather than the thermal modeling of the human body. Therefore, the model can be simplified as long as it produces an accurate device performance. We validated the accuracy of the simplified version through a comparison with the available experimental data. The guidelines presented in this work can be easily implemented in commercially available FEM software such as ANSYS or COMSOL. Apart from thermoelectric applications, applications such as wearable sensors that measure the thermal properties of the skin [22, 23] can vastly benefit from the modeling guidelines presented in this paper. Furthermore, we present performance of thermoelectric device coupled with a simplified human thermoregulatory model to show the variations in the results when the skin is not properly modeled. By doing so importance of considering human thermoregulatory model when designing wearable thermoelectric devices are highlighted. Errors caused by the wrong prediction of skin thermal actually can be large enough even override the actual thermoelectric effects (Seebeck effect, Peltier effect and Joule Heating). Even device heat sink performance can be altered by the thermoregulatory model which illustrates by conducting numerous simulations varying convective heat transfer coefficient.

2. Simplified human thermoregulatory model

For wearable thermo-electrical simulations, the thermal properties of a local area of the skin are sufficient to obtain accurate results. Therefore, existing human models need to be adjusted to some extent for use in local body parts. Herein, we approximated the core body temperature near the required body part, and in so doing, the modeling of the skin becomes a simple and straightforward task. Otherwise, a simulation of the entire human body is needed to obtain the core body temperatures of a certain location, which are quite impractical when the simulations are focused on certain applications. To determine skin thermal properties in a certain skin layer, an understanding of thermoregulation of all parts of the human body at the same time is required. We simplified the human thermoregulatory system such that not all parts of the human body need to be considered.

From the modeling perspective, the human thermoregulatory system can be separated into two types: passive and active systems[19]. The passive system is the internal and external heat transfer part of the model, and the active system is the thermal control and response part. Active system controls the passive system to maintain thermally comfortable conditions for the body and internal organs. Basically, the active system employs four strategies to regulate the temperature inside the body: (i) control of the blood volume flow rate through the skin tissues, (ii) evaporation, (iii) control of the local metabolic heat generation, and (iv) shivering (see Figure 1)

2.1. Geometry

Modeling of the passive system begins with a geometrical construction of the body parts. As illustrated in Figure 1, in human thermoregulatory modeling simulations, human body parts are simplified as cylindrical objects formed through the stacking of different types of tissue layers: bone, brain, viscera, lung, muscle, fat, dermis, and epidermis. The existence of each tissue type and its proportion strongly depends on the region of the body considered. Therefore, accurate physiological data of a certain body part are required to construct the simulation model. Geometrical and physiological information on the body parts can be found in various research materials [17, 19, 20, 24].

In this paper, the forearm, forehead, and volar forearm (wrist) are modeled and simulated. The physiological data required were obtained from Fiala *et al*.[19] and Wilson *et al*.[25]. The volar forearm was chosen mainly because it is the most commonly preferred location for wearable devices. Thus, all thermoelectric simulations described in this paper were conducted on the volar forearm. Additionally, for verification purposes, the forehead and forearm were simulated and the results are compared with existing experimental results.

2.2. Heat transfer modeling in tissue

Normally, in biological tissue, heat is generated through the metabolic process, and heat is exchanged through blood circulation. However, these processes occur only in specific types of biological tissue. For example, in the volar forearm, fat and epidermal tissues do not have a considerable blood supply, but the muscle and dermal tissues have a considerable blood flow and a good metabolic heat generation. Modeling such tissues require an equation that takes into account the heat exchange process with blood. As a solution, Pennes et al.[12], introduced a simple modified conduction equation by adding a blood perfusion term to the conventional conduction equation. This modified equation is also referred to as the Pennes bioheat transfer equation, which is a simplified case of an actual complex heat transfer that occurs from blood flowing through the tissues.

$$K\left(\frac{\partial^2 T}{\partial x^2}+\frac{\partial^2 T}{\partial y^2}+\frac{\partial^2 T}{\partial z^2}\right)+q'''_m+c_b\dot{m}v_{bl}\left(T_{bl}-T_{ti}\right)=\rho c\frac{\partial T}{\partial t} \tag{1}$$

$$c_b\dot{m}v_{bl}(T_{bl}-T_{ti})=\rho_{bl}c_b\omega(T_{bl}-T_{ti}) \tag{2}$$

Equation (1) is the basic governing equation for the three-dimensional heat transfer in all tissues. The volumetric blood flow rate through the tissue is denoted by $\dot{m}v_{bl}$ [kg/m^3-s], the metabolic heat generation of the tissues is denoted by q'''_m [W/m^3], and the heat capacity of the blood is given by c_b [J/kg-K]. According to the Pennes equation, blood enters the tissue with the blood temperature, T_{bl}, of that location, and leaves the tissue with tissue temperature, T_{ti}. Thus, in the Pennes bioheat equation, the maximum heat exchange between blood capillaries and tissues are assumed. As shown in equation (2), the blood flow rate in the Pennes equation is represented by the blood perfusion term, ω [1/*s*]. The blood perfusion value is highly variable and is the main control function regulating heat inside the body. As illustrated in Figure 1, an increase in the blood flowrate through the skin is known as vasodilation, and a reduction of the blood flow rate is known as vasoconstriction. Variations in the blood flow rate are accomplished through the expansion and constriction of the capillary tubes. Hence, in a mathematical modeling of the skin, a variable blood flow rate, $\dot{m}$, needs to be considered. In dermal tissue, a variable blood flow rate occurs owing to the regulation of the temperature. Thus, when applying the Pennes bioheat equation (equation (1)) for the dermis, the vasodilation and vasoconstriction functions need to be considered.

$$\dot{m}_{skin,dil} = \begin{cases} \dot{m}_{skin,basal}; & T_{core} \leq 36.8 \\ \left(\dfrac{T_{core} - 36.8}{37.2 - 36.8}\right)\left(\dot{m}_{skin,\max} - \dot{m}_{skin,basal}\right) + \dot{m}_{skin,basal}; & 36.8 \leq T_{core} \leq 37.2 \\ \dot{m}_{skin,\max}; & T_{core} \geq 37.2 \end{cases} \quad (3)$$

$$\dot{m}_{skin,con} = \begin{cases} \dot{m}_{skin,\min}; & T_{skin} \leq 27.8 \\ \left(\dfrac{t_{skin} - 27.8}{33.7 - 27.8}\right)\left(\dot{m}_{skin,basal} - \dot{m}_{skin,\min}\right) + \dot{m}_{skin,\min}; & 27.8 \leq T_{skin} \leq 33.7 \\ \dot{m}_{skin,basal}; & T_{skin} \geq 33.7 \end{cases} \quad (4)$$

$$\dot{m}_{skin} = \frac{\dot{m}_{skin,dil} . \dot{m}_{skin,\text{con}}}{\dot{m}_{skin,basal}} \quad (5)$$

In this work we have used the work by Salloum *et al*.[26] to model vasodilation and vasoconstriction functions. The functions proposed by Salloum *et al*. have the advantage of being simple compared to those of the Fiala model with exhibiting good accuracy. Vasodilation is a function (equation (3)) of the core body temperature, T_{core}, and vasoconstriction (equation (4)) is a function of the skin temperature, T_{skin}. The total blood flow rate is a combination of both the vasodilation and vasoconstriction functions, and is given by equation (5)[26]. For muscle tissue, variations in the blood flow rate are a function of the activity level of the muscle group rather than thermal regulation. A constant blood flow rate through the muscle can be assumed when the muscle group is not conducting a considerable amount of physical activity.

2.3. Heat loss mechanisms

Heat loss mechanisms are critical to the human body, preventing the internal organs from failing owing to a rise in core body temperature. Convection, radiation, and evaporation are the heat loss mechanisms that occur at the surface of the skin. Convection and radiation are uncontrollable and dependable functions of the ambient conditions. On the contrary, evaporation is a fully controllable function triggered at elevated skin and core temperatures. Thus, evaporation can be considered a part of an active system.

Convective heat flux (q_c'') between the skin surface and ambient air can be calculated by applying Newton's law of cooling, as stated in equation (6). Here, skin and ambient temperatures are denoted by T_{skin} and T_a respectively.

$$q_c'' = h_{skin}\left(T_{skin} - T_a\right) \tag{6}$$

The heat transfer coefficient, h_{skin}, should be calculated experimentally for the skin surface owing to its unique surface roughness and hair shaft mechanism. Human skin is designed to trap a thin layer of air for the purpose of providing additional insulation. The thickness of this air layer is regulated by the hair shaft mechanism. Under cold conditions, the hair shaft become straighter to increase the air layer thickness. Conversely, under hot conditions, it becomes more parallel to the skin, reducing the thickness of the air layer. Thus, the heat transfer coefficient becomes a function of the skin and ambient temperatures. Additionally, it shows an obvious variation with the effective air velocity and location of the body part. A sufficient amount of research has been conducted on the parametric dependency of the heat transfer coefficient of human skin[27-29]. In this paper, the heat transfer coefficient of the skin surface is based on an equation by Fiala *et al*.[19], which was derived from experimental data by Wang *et al*.[30-32], which is

$$h_{skin} = \sqrt{a_{nat}\sqrt{T_{skin} - T_a} + a_{frc}V_a + a_{mix}} \tag{7}$$

where constants a_{nat}, a_{frc} and a_{mix}, in equation (7) are fitting parameters and have constant values based on the location of the body. Fitting values used for the simulations are provided with the appendix (Table 1).

Following equation was used based on the assumption that the human arm is small compared with the surrounding enclosure. The radiative heat flux, q_r'', is given by

$$q_r'' = \varepsilon\sigma\left(T_a{}^4 - T_{skin}{}^4\right) \tag{8}$$

The skin surface emissivity and Stephan Boltzmann constant are given by ε and σ, respectively. Owing to high emissivity of both skin[33] (ε ~ 0.94 to 0.98) and fabric[34] (ε ~ 0.9), radiation loss is not considerably smaller compared to heat loss due to convection. Human skin always contains some level of moisture, and thus evaporation always occurs under all types of conditions. When the skin temperature becomes high, sweat glands release extra water to the epidermis, thereby increasing the heat loss through evaporation. The amount of released water is a function of the skin and core temperatures. In this work, sudomotor functions in the Smith model was used to simulate evaporation. From equation (9) [17], the sweat threshold temperature, T_{sweat}, can be calculated. From equation (9)[17], From equation (10)[17], the amount of sweat mass released, $\dot{m}_{sw}$, by the sweat glands can be calculated.

$$T_{sweat} = \begin{cases} 42.084^o C - 0.15833 T_{skin}; & T_{skin} < 33.0^o C \\ 36.85^o C; \quad T_{skin} \geq 33.0^o C \end{cases} \tag{9}$$

$$\dot{m}_{sw} = \frac{45.8^o c + 739.4(T_{core} - T_{sweat})}{3.6x10^6 (C^o.s.kg^{-1})}; \quad T_{core} > T_{sweat} \tag{10}$$

A dimensionless parameter, skin wettedness, w, is introduced to express the total moisture level in the epidermis by adding the existing moisture level to the generated sweat mass. Skin wettedness can have a value up to unity depending on the sweat generation rate. Wettedness can be expressed as equation (11)[17]. The evaporative heat flux, q_e'', can be calculated from equation (12)[17]. According to equation, minimum value can be 0.06 because evaporation occurs even under cold conditions owing to the moisture level of the epidermis.

$$w = 0.06 + \frac{1 - 0.06}{0.000193 kg / s}\dot{m}_{sw} \tag{11}$$

$$q_e'' = \frac{w\left(p_{sk} - p_a\right)}{\left[\mathrm{R}_{e,cl} + \frac{1}{f_{cl}h_e}\right]} \tag{12}$$

As expressed in this equation, q_e'' becomes a function of ambient conditions such as the humidity and properties of the clothing worn, such as the evaporative heat transfer resistance of the clothing, $R_{e,cl}$, the clothing area factor, f_{cl}, and the effective heat transfer coefficient, h_e. The equation is also function of water vapor pressure, P_{sk}, at water vapor pressure of ambient temperature, P_a. Ambient water pressure is directly related to ambient air and humidity.

2.4. Control of local metabolic heat generation and shivering.

Shivering and variable metabolic heat generation are critical under special conditions such as extreme cold weather and during physical activities. In this work, the shivering effect is neglected because it occurs under special conditions such as relatively low core body temperatures. The metabolic heat generation, q'''_m, can be expressed as equation (13)[19].

$$q'''_m = q'''_{m,basal} + q'''_{m,basal}[2^{(T_{ti}-T_{set})/10} - 1] + q'''_{m,shiver} + q'''_{m,work} \tag{13}$$

$$q'''_{m,work} = \frac{\partial(a_m \cdot WH)}{\partial V_{mus}} \tag{14}$$

Deviation from the tissue temperature, T_{ti}, under thermo-neutral tissue conditions, T_{set}, directly influences the basal metabolic heat generation ($q''_{m,basal}$) as shown in the second term of equation (13). Here, $q''_{m,work}$ is the contribution to the metabolic heat generation by exercising. We only consider a constant metabolic heat generation in tissue. Heat generation through shivering ($q''_{m,shiver}$) is also neglected because it only occurs in extreme weather conditions. Here, WH denotes workload in watt of the whole body and a_m is a distributing coefficient of a body part so that a_m multiplied by WH indicates metabolic rate in the specific body part under consideration. In equation (14), V_{mus} is the muscle volume of the body part.

3. Numerical analysis of human skin using human thermoregulatory system

A simple simulation model was constructed following the guidelines presented in the previous sections for the volar forearm, as illustrated in Figure 1. The physiological details and blood flow rates of the volar forearm are given with the appendix (Table 1). The model requires the blood temperature of the desired location and the core body temperature as input values. For most cases, the core and blood temperatures can be approximated, especially when the body is in a thermo-neutral state. For a thermo-neutral state, the core body temperature is around 37 °C[35]. The blood temperatures of the organs and parts closer to the core of the body can be assumed as being similar to those at the body core. For parts such as the arms and legs, an obvious temperature drop from the core temperature occurs in most cases. Chato *et al*.[36] presented a method for calculating the temperature drop of the blood in the arm, which can be used as a guideline to calculate the temperature drop accurately. According to Chato's calculations, a temperature drop of 2 °C can be possible in the arm. In this paper, for the forearm and volar forearm, we considered a 1 °C drop in the blood temperature from the core body temperature under all conditions, and for the forehead we considered the blood temperature to be equal to the core body temperature. The core body temperature is taken as 37 °C[35], which is a normal value when the body is in a thermoneutral state. Bone tissue is considered to be in a constant temperature state and its temperature is the same as the blood temperature at a particular location.

3.1 Summary of simplification in the human thermoregulatory model

Geometrical modeling of the human body presented in the work presents simplified version of the well-established human models [16, 17, 35]. Radiative heat transfer was modeled under assumption of human arm is small compared with the surrounding enclosure.

Evaporative heat transfer is (equations (9), (10), (11), and (12)) based on the work by Smith *et al*.[17], since the Smith's evaporative functions adequately explain experimental data. For more accurate expression, one can use the functions proposed by Fiala *et al*[19]. Expression on convection heat transfer (equations (6) and (7)) was adopted by the Fiala model [19], which matched well with experimental data by Wang *et al* [30, 31]. Heat transfer in tissues was modeled by the Pennes's bio heat equation (equation (1)). Variable blood flow rate was adopted from Salloum *et al*.' expression[26] (equations (3), (4) and (5)) which assumed linear variation in perfused blood flow rate. Other models such as Fiala *et al*.[19] considered hypothalamus functions, which is not required for estimating skin thermal resistance for body heat harvesting. The shivering effect is neglected because it occurs under special conditions such as relatively low core body temperatures. Core temperature of the body is assumed to be constant and set to be 37 °C which is a normal value for thermos-neutral state[35]. Change in the core temperature should be considered in certain situation – for example, when a person is located in either very hot or cold environment.

4. Verification of human thermoregulatory model

To validate the developed simulation model, the results were compared with experimental data. Experimental data related to skin temperature are highly abundant. Munir *et al*.[37] conducted experiments on the skin temperature variation with respect to time under different ambient conditions. For this study, we used the experimental data obtained by Munir *et al*.[37] to validate our simulation model. Transient simulations were conducted following the same external conditions as in Munir's experiment, which are illustrated in Figure 2. As shown in Figure 2, both the forehead (b) and forearm (c) simulation results show good agreement with the experimental data which justify the accuracy of the simulation process. The developed model contains functions from of Fiala model and Smith model. Therefore, simulation results[37] from those models are also integrated into the same plot for comparison. As shown in the Figure 2, our model matches adequately to those models, which presents reliability of our developed model. However, slight deviation among models might be caused by variation in core temperature or use of different blood perfusion functions.

5. Skin thermal characteristics

Simulations are also conducted to calculate important thermal parameters such as heat flux, skin temperature and skin thermal resistance. Figure 3 illustrates the variation in skin thermal properties in the volar forearm with respect to ambient temperature and heat transfer coefficient. In the simulation, the relative humidity (RH) of 40%, and core temperature of 37 °C were considered. In real applications, any factor affecting on the heat loss from the skin could alter its thermal characteristics. Here, we only illustrate the variation of skin thermal properties according to ambient temperature and heat transfer coefficient, mainly because these are the most general variables affecting the skin thermal properties. As illustrated in Figure 3(a), heat flux through the skin reduces with the increase of ambient temperature and increases with increasing heat transfer coefficient. Therefore, heat flow through the skin is highly dependent on the ambient conditions because it controls the heat loss from the skin surface. For the given conditions heat flux variation of 100-950 W/m^2 is visible near the volar forearm. Considering the heat flux through the skin is also critical. Having higher heat flow rates through the skin can be uncomfortable for many people under normal conditions. Heat fluxes of over 250 W/m^2 are known to be uncomfortable[37] for many people under basal conditions. Therefore, it is critical to pay attention to the heat flux when designing a device. Figure 3(b) illustrates the skin temperature variation in same conditions. Skin temperature increases with the increasing ambient temperature and decreases with increasing heat transfer coefficient. Skin temperature variation of 10-34 °C was obtained for volar forearm in simulated conditions. As illustrated, skin temperature drops with the increasing heat flux, which is an obvious phenomenon in such situations. Change of thermal resistance of the skin more emphasizes the effect of human thermoregulatory as visible in skin thermal resistance graph in Figure 3(c). Thermal resistance is fluctuating due to the effect of thermoregulatory system. For high heat transfer coefficients, rapid skin temperature fluctuation with ambient conditions occurs, therefore, abrupt change in thermal resistance is observed. According to equation (4), vasoconstriction function of the thermoregulatory system reduces the blood flow rates to minimum when tissue temperature reaches values below 27.8 °C. Due to this reason, the rapid increase of thermal resistance in lower ambient temperature is noticed. While, in higher ambient temperatures, blood flow rates increase accordingly and reduce the thermal resistance facilitating the heat loss through the body. In this case, we have used core body temperature of 37°C, but for higher core body temperatures blood flow rates would increase further and reduce the skin thermal resistances. The thermal resistance of the skin was calculated by dividing the temperature difference between the skin and the core temperature of the location from the heat flux through the skin. The obtained thermal resistance of the skin is therefore is a virtual value, which is used to express the variable heat transfer in the skin. In an actual case, the thermal properties such as the thermal conductivity and heat capacity remain unaffected.

6. Wearable thermoelectric device

In a wearable thermoelectric generator (TEG), the temperature gradient between the skin and ambient air is utilized to generate electrical power. On the other hand, wearable thermoelectric refrigerator (TER) devices, exploit the cooling effect in thermoelectric materials when they are subjected to electric current.

To understand the role of a human thermal model in a wearable thermoelectric generator or refrigerator, an analytical model for calculating the power output from the device is first discussed. In Figure 4(a) basic components of thermoelectric unit couple are illustrated. The domain of the unit couple was chosen as possible to be repeated up to fully scaled device. Unit couple consists of *p* and *n* thermoelectric elements, filler materials and heat sink. The power generated by the thermoelectric generator can be estimated simply using equation (15) [38]:

$$P = \frac{V^2}{R_L}\frac{m^2}{(1+m)^2} \tag{15}$$

Here, V is the voltage of the thermoelectric generator, m is the load electrical resistance (R_L) to device internal electrical resistance ratio. The maximum power occurs when the load resistance is equal or closer to the internal resistance of the device[38]. For maximum power, m is equal $\sqrt{ZT+1}$[39]. ZT is the thermoelectric figure of merit of the thermoelectric material. In this work, by doing repetitive simulations for number of m values, optimum m value was calculated. However there are many works on how to calculate optimum m directly which is not discussed here[40]. Voltage is a function of the temperature difference between the thermoelectric elements, and can be expressed as shown in equation (16)[38]:

$$V = n(S_n + S_p)\Delta T \tag{16}$$

Using equation (15) and (16), the power output can be calculated approximately if the temperature difference across the device (ΔT) is known. Here, S is the Seebeck coefficient of the material, and n is the number of elements in the device. To calculate the temperature difference in the device, a simple thermal resistance network of the unit couple was constructed. Thermal resistance network for single unit couple is illustrated by Figure 4(b). Using the thermal resistance network, an expression for the temperature difference across the thermoelectric element can be obtained, as given in equation (17).

$$\Delta T = T_{TEG,H} - T_{TEG,C} = \frac{\left(\frac{1}{R_{t,TEG}} + \frac{1}{R_{t,Fill}}\right)^{-1}}{\left(\frac{1}{R_{t,TEG}} + \frac{1}{R_{t,Fill}}\right)^{-1} + R_{t,C} + R_{t,contact} + R_{t,skin}} \left(T_{core} - T_a\right) \tag{17}$$

According to the equation (17), temperature difference of the thermoelectric element is a direct function of thermal resistance of human skin, $R_{t,skin}$. Hence it becomes function of the generated power. Thus, by accurately modeling the human skin, a more realistic device performance can be simulated. However, thermal resistance of the thermoelectric elements ($R_{t,TEG}$) is variable due to Peltier effect when the device is operating. In this reason, an effective thermal conductivity concept when calculating thermal resistance of the device is suggested given in equation (18)[40, 41], where K is material thermal conductivity, L is the element height, and A is the element area.

$$R_{t,TEG} = \frac{KA}{L}\left(1 + \frac{ZT}{1+m}\right) \tag{18}$$

Although solution for wearable thermoelectric devices can be solved analytically, simulations presented in the paper are all done using numerical methods with the aid of Comsol Multiphysics software.

Unlike thermoelectric generators, wearable thermoelectric refrigeration devices are less familiar. However, they could have a considerable importance and popularity in the future with the development of flexible and efficient thermoelectric materials. Thus, we included simulation on a wearable thermoelectric refrigerator (TER).

$$\frac{d^2T}{dx^2} - \frac{hp_r}{KA}(T - T_a) + \frac{\rho_e j^2}{K} = 0 \tag{19}$$

$$-K\left.\frac{dT}{dx}\right|_{x=0} + ST_{\mathrm{TEC,C}}\, j = q''_{human} \tag{20}$$

$$-K\left.\frac{dT}{dx}\right|_{x=l} + ST_{TEC,h}\, j = h_c(T_{TEC,c} - T_a) \tag{21}$$

In thermoelectric refrigeration (TER), analytical solutions are derived by considering the energy balance of the hot and cold sides of the system. equation (19) consists of heat conduction, heat convection, and joule heating terms obtained through an energy balance of the total system. The boundary conditions of the TER can be expressed as shown in equation (20) and (21). One side of the TER is subjected to the heat input from the skin, q''_{human}, and on the other side, the heat is dissipated through convection. As expressed in equation (20), TER is directly coupled with the heat flux of the skin. Therefore, refrigeration power and power consumption of the device depend highly on resistance of human skin.

7. Simulation results of wearable thermoelectric devices

In this section wearable device combined with human model simulations are discussed. The material and geometrical properties of the unit couple are shown in appendix (Table 2). The simulations were conducted by considering the device placed on the volar forearm. Here, a filler material with a thermal conductivity of 0.21 W/m K was used, which is common value for most flexible polymer fillers. For the TEG simulations, an ambient temperature of 20 °C, heat transfer coefficient of the heat sink of 20 W/m^2 K, relative humidity of 40%, and core temperature of 37 °C were taken as the set conditions. Based on the numerical simulation results, the power output of the device can be calculated similar to equation (15). Figure 5(a) displays the temperature difference across the thermoelectric element respect to fill factor and also it displays device electrical conductance variation with the fill factor. Fill factor is the percentage of thermoelectric material in the device. Temperature difference across thermoelectric element is reduced with the increase of fill factor because the filler material has lower thermal conductivity than that of thermoelectric material. On the other hand, the device conductance is increased with fill factor due to the increase of conducting area of the element. Temperature difference of the element is plotted for three estimated skin thermal resistance values which have used in recent articles related to wearable thermoelectric devices (0.0135 m^2 K/W[7], 0.02 m^2 K/W[8], and 0.0666 m^2 K/W [9]) as shown in Figure 5(a). Skin thermal resistance simulated by the simplified human model can vary its resistance, which is referred as variable-skin-thermal-resistance model (VRM), whereas, when skin thermal resistance does not change irrespective of environmental condition, we denote it as constant-skin-thermal-resistance model (CRM).

According to the Figure 5, temperature difference obtained based on the CRM of 0.0666 m^2 K/W shows large deviation compared to values predicted by human model simulations. The other two cases (0.0135, and 0.02 m^2 K/W) based on the CRM shows little deviation suggesting actual skin thermal resistance is somewhat closer to 0.02 m^2 K/W.

For the optimum power output, high temperature difference and high device conductance is preferential. Therefore, simulations are usually required to find the optimum filler percentage of a certain device under particular conditions. Based on the filler percentage, the power output can be increased or decreased, as shown in Figure 5(b). The effect of filler percentage on power output can be understood by observing analytical equation (17). Similarly, we have analyzed the optimum filler percentage of the device using different thermal resistances of the skin. As illustrated in Figure 5(b), the optimum filler percentage does not show a significant variation with the chosen thermal resistances of the skin, but the maximum power output has values showing noticeable deviation with the skin thermal resistance. The maximum power output changing with the thermal resistance of the skin suggests that the heat flux through the thermoelectric element is altered. The optimum filler percentage should change with the alternating heat flux; however, the change in filler percentage will also alter the electrical resistance of the device, and therefore the overall optimum point of the fill factor has shown unnoticeable change.

Next, we considered the TEG with an improved heat sink performance. Using a high-performing heat sink is one of the main methods for enhancing the performance in the TEG and TER. In Figure 6(a), the power output of the device corresponding to the heat transfer coefficient, h_c, in the heat sink is illustrated. According to Figure 6(a), increasing heat transfer coefficient to over 100 W/m^2 K has shown a smaller change in power output corresponding to the heat transfer coefficient of the heat sink, as illustrated by the simulation line representing human model. The main reason for this is an increase in the thermal resistance of the skin due to higher convection rates by the human thermoregulatory system to reduce heat loss. Thus, having a larger heat sink would not increase the performance as much as expected because the thermal resistance of the skin can also increase. Therefore, a human model can also be extremely beneficial in designing a heat sink for wearable devices. Figure 6(b) illustrates the deviation of power output between three constant resistance models and human model. For the lower heat transfer coefficient conditions, the graph of 0.02 m^2 K/W shows the least amount of deviation, indicating that the actual thermal resistance of the skin is somewhere closer to 0.02 m^2 K/W. However, after increasing h_c deviation increases, indicating that the skin resistance also changed under higher convective heat transfer conditions. According to Figure 6(b), the deviation in the percentages shows an error large 50 to 65% can occur when the thermal resistance of the skin is modeled as 0.0666 m^2 K/W .Which is a great example where results can be extremely erroneous when wrong skin thermal resistance values being used. Similarly, the graph for a 0.02 m^2 K/W resistance of the skin also shows an error of 15% in higher heat transfer coefficients. Therefore, a large percentage-wise deviation in power output can be observed. Even for the moderate heat transfer coefficients error of 5-10% could occur which is quite large deviation in the context of thermoelectric devices.

Unlike thermoelectric generation, a variable thermal resistance of the skin can have a much higher value on the thermoelectric refrigeration. In thermoelectric refrigeration, the skin temperature consistently changes by the thermoelectric refrigerator (TER) due to heat removal from the skin, which often results in a highly fluctuating thermal resistance of the skin. The TER performance was also analyzed using two unit couples similar to the TEG by varying the convective heat transfer coefficient of the heat sink and the ambient temperature. The device is considered to be placed on the volar forearm, moderate electric current of 1.2A is supplied to the device, and the ambient temperature is considered to be 35 °C.

In previous study we have shown that skin thermal resistance is likely to be falls around 0.02 m^2 K/W Therefore we have chosen four skin thermal resistance values (of 0.015, 0.02, 0.025, and 0.03 m^2 K/W) to compare with human model results. Figure 7(a) illustrates the reduction in skin temperature using TER, corresponding to the convective heat transfer coefficient of the heat sink of the device. In Figure 7(a), the thermal resistance graph for 0.025 m^2 K/W has the closest deviation with the human models simulations results at lower heat transfer coefficients, indicating that the actual thermal resistance of the skin is close to 0.025 m^2 K/W at low heat transfer coefficients. With further rise in heat transfer coefficient the “VRM” line deviate further away and become close to 0.03 m2 K/W. According to Figure 7(a), when the thermal resistance of the skin is considered to be 0.015 m^2 K/W, a maximum temperature drop of 3 °C can be achievable. However, in an actual case, a maximum temperature drop of nearly 5 °C can be reached under the given conditions. Thus, this clearly emphasizes that an improper modeling of the skin can show a high deviation in the results from the practically obtainable values. Figure 7(b) represent the heat flux from the device for same conditions. According to the figure, when skin thermal resistance is 0.015 m^2 K/W which is smaller than that based on the VRM, the calculated heat flux from the skin is higher than heat flux based on the VRM which underestimate the device capability. On the other hand, when skin thermal resistance is 0.03 m^2 K/W, calculated heat flux from the skin is lower than heat flux based on the VRM which overestimate the device capability. Another important factor based on the

Figure 7(a) and Figure 7(b) is that increasing heat sink's heat transfer coefficient is not effective over a certain value. According to the graphs the heat transfer coefficient over 50 $W/m^2 K$ does not result in large decrease of skin temperature. Therefore, just like for power generation applications, the human thermoregulatory model can assist to design optimized heat sink in designing TER. Optimized design of heat sink is very critical mainly because it will occupy large area and also consume considerable portion of manufacturing cost. So, by optimizing the heat sink the cost reduction, aesthetic look and performance can be controlled. Finally, we considered a constant thermal resistance value of 0.021 $m^2 K/W$ to compare with the human model under initial conditions of 35 °C in ambient temperature and 40% relative humidity, which is illustrated in Figure 8(a) and Figure 8(b). Initially both models have thermal resistance of 0.021 $m^2 K/W$. Therefore, the initial skin temperatures of both models are the same. With the increase in supplied current, the skin temperature drops, as shown in Figure 8(a). The human model (VRM) shown a higher temperature reduction compared to constant resistance model with 0.021 m2 K/W (CRM). With the skin temperature reduction thermal resistance of the skin increases resulting higher temperature deviation between VRM and CRM. Here also VRM is capable achieving higher temperature drop compared to CRM mainly because of the change in skin thermal resistance. Similarly heat flux from the skin is increased with the increasing electric current due to refrigeration of the device. Difference between the two models also increases respect to the supplied electric current. The reason for this is that the body minimizes the blood flow rate to control the heat loss therefore thermal resistance of the skin increases. Figure 8(b) illustrates the power consumption of the device with respect to the temperature drop of the skin. Constant resistance models show higher power consumption compared to a variable resistance model when obtaining the same temperature drop. Therefore, in refrigeration simulations, assuming constant thermal resistance conditions can often result in an underestimation or overestimation the performance.

8. Conclusions

The human thermoregulatory system is designed to regulate the heat inside the body. Therefore, it uses control functions such as the blood flow rate and evaporation to maintain the heat loss. This behavior causes a change in heat output from the skin. In this paper, we presented a non-rigorous but accurate method to model the thermal resistance of the human skin in the context of designing efficient wearable and/or implantable devices. Wearable thermoelectric generation (TEG) and refrigeration (TER) devices are simulated to illustrate the fluctuations in performance based on the thermal resistance of the skin. We showed a fluctuation in the thermal resistance of the skin under main external conditions, and how the performance of the thermoelectric devices fluctuates depending on this thermal resistance. For thermoelectric power generation, it can be as large as 60%. For refrigeration application, constant thermal resistance is not especially suitable because the skin temperature keeps changing due to the refrigeration effect. For example, as shown in Figure 7(a), device can reach a temperature drop of 5 °C. However, in some cases, when an inaccurate thermal resistance of the skin has been used for simulations, the results have shown that the device is unable to reach such a temperature difference. This can often lead to an unnecessary over design or under design of the device to reach the required temperature drop. However, the performance of thermoelectric material is still not at a desirable level, and therefore, a change in the thermal resistance of the skin might not have an impact on the outcome of the device in certain cases. In the future, more improved thermoelectric materials will be developed, which can lead to further variation of device performance with the human thermoregulatory system. Therefore can come to the conclusion that human thermoregulatory system plays important role, as same as thermoelectric effects does in (Seebeck, Peltier and Joule heating) dictating the performance of wearable thermoelectric devices.

Acknowledgement

This work was supported by the National Research Foundation of Korea (NRF) Grant funded by the Korean Government (MSIP) (NRF-2015R1A5A1036133).

Nomenclature

Description	Units	Symbol
Thermal conductivity	W/m K	K
Density	kg/m^3	ρ
Blood perfusion	1/s	ω
Heat generation	W/m^3	q'''_m
Volumetric blood flow rate	kg/m^3 s	$\dot{m}v_{bl}$
Tissue temperature	^{o}C	T_{ti}
Blood temperature	^{o}C	T_{bl}
Heat capacity	J/kg K	c_b
Blood density	kg/m^3	ρ_{bl}
Ambient temperature	^{o}C	T_a
Heat transfer coefficient of skin	W/m^2 K	h_{skin}
Skin temperature	^{o}C	T_{skin}
Convection heat flux	W/m^2	q''_c
Regression coefficients for natural		a_{nat}
Regression coefficients for forced		a_{frc}
Regression coefficients for absolute		a_{mix}
Effective velocity of air	m/s	V_a
Emissivity		ε
Boltzmann constant temperature	W/m^2 K^4	σ

Radiation heat flux	W/m^2	q''_r
Core temperature	^oC	T_{core}
Mass flow rate of vasodilation	kg/s	$\dot{m}_{skin,dil}$
Mass flow rate of vasoconstriction	kg/s	$\dot{m}_{skin,con}$
Mass flow rate of basal skin	kg/s	$\dot{m}_{skin,basal}$
Maximum mass flow rate of skin	kg/s	$\dot{m}_{skin,\max}$
Minimum mass flow rate of skin	kg/s	$\dot{m}_{skin,\min}$
Total mass flow rate of skin	kg/s	$\dot{m}_{skin}$
Threshold temperature of sweating	^oC	T_{sweat}
Amount of sweat mass	kg/s	$\dot{m}_{sw}$
Wettedness		w
Saturated water vapor on skin	Pa	p_{sk}
Ambient water vapor pressure	Pa	p_a
Clothing resistance	m^2 Pa/W	$R_{e,cl}$
Clothing area factor		f_{cl}
Evaporative heat transfer coefficient	W/m^2 Pa	h_e
Evaporative heat flux	W/m^2	q''_e
Setting temperature of tissue	^oC	T_{set}
Basal metabolic heat generation	W/m^3	$q'''_{m,basal}$
Shivering metabolic heat generation	W/m^3	$q'''_{m,shiver}$
Extra exercising metabolic heat generation	W/m^3	$q'''_{m,work}$
Body part wise distributing coefficient of extra metabolism		$a_{m,WH}$
Body-element muscle volume	$1/m^3$	V_{mus}
Maximum power	W	P_{max}
Open circuit voltage	V	V_{oc}
Load resistance	Ω	R_L
Number of elements		n

Temperature difference between TEG	K	ΔT
Seebeck coefficient of n-type	V/K	S_n
Seebeck coefficient of p-type	V/K	S_p
Hot side temperature of TEG	ºC	$T_{TEG,H}$
Cold side temperature of TEG	ºC	$T_{TEG,C}$
Thermal resistance of TEG	m^2 K/ W	$R_{t,TEG}$
Thermal resistance of filler	m^2 K/W	$R_{t,Fill}$
Thermal resistance of cold side	m^2 K/W	$R_{t,C}$
Thermal resistance of contact	m^2 K/W	$R_{t,contact}$
Thermal resistance of skin	m^2 K/W	$R_{t,skin}$
Figure of merits		ZT
Electrical load resistance ratio		m
Height of thermoelectric element	m	L
Perimeter of TEC	m	p_r
Cross section area of TEC	m^2	A
Electrical resistivity	Ω m	ρ_e
Current density	A/m^2	j
Cold side of TEC	ºC	$T_{TEC,C}$
Hot side of TEC	ºC	$T_{TEC,H}$
Human heat flux	W/m^2	q''_{human}
Heat transfer coefficient of heatsink	W/m^2 K	h_c

Appendix

Table 1. Geometrical data for modeling body parts (Volar forearm, Forearm and Forehead)

Description	units	Volar forearm[25]	Forehead[19]	Forearm[19]
Geometrical data				
Thickness of muscle	m	0.0068	0.0138	0.019
Thickness of fat	m	0.002	0.008	0.0058
Thickness of lower dermis	m	0.0005	0.001	0.0005
Thickness of upper dermis	m	0.0006	0.0009	0.0011
Thickness of epidermis	m	0.0001	0.0001	0.0001
Thermal conductivity of muscle	W/m K	0.53	0.53	0.42
Thermal conductivity of fat	W/m K	0.16	0.16	0.16
Thermal conductivity of lower dermis	W/m K	0.53	0.53	0.47
Thermal conductivity of upper dermis	W/m K	0.53	0.53	0.47
Metabolic rate of muscle[19]	W/m^3	703.5	684	684
Metabolic rate of skin[35]	W/m^3	1010	368	368
Blood flow rates and other data[19]				
Basal blood flow rate per tissue	$10^{-9} m^3/kg\ s$	542	6709	542
Min blood flow rate per tissue mass	$10^{-9} m^3/kg\ s$	0	5295	0
Max blood flow rate per tissue mass	$10^{-9} m^3/kg\ s$	4306	11079	6455
a_{nat}[19]		8.3	3	8.3
a_{fr}[19]		216	113	216
a_{mix}[19]		-10.8	-5.7	-10.8
Emissivity of human skin		0.98		
Relative humidity		40%		

Table 2. Simulation data for thermoelectric generation and refrigeration device

Description	Units	Value(TEG)	Value(TER)
Thermoelectric element			
Width	m	0.005	0.005
Depth	m	0.005	0.005
Height	m	0.006	0.006
Thermal conductivity of p-type	W/m K	0.88716	0.88716
Thermal conductivity of n-type	W/m K	0.95801	0.95801
Thermal conductivity of gap filler	W/m K	0.21	No filler
Seebeck coefficient of p-type	V/K	-0.000170	-0.000170
Seebeck coefficient of n-type	V/K	0.000252	0.000252
Electrical conductivity p-type	S/m	50765	50765
Electrical conductivity n-type	S/m	71925	71925
Simulation conditions			
Total area of heat sink	m^2	0.0002	0.0002
Emissivity of heat sink		0.5	0.5
Number of unit couples		1	2
Ambient temperature	C	20	35
Relative humidity		40%	40%
Heat transfer coefficient in heat sink	W/m K	20	30
Interface thermal contact resistance[9]	m^2 K/W	0.02	0.02
Input current	A		1.2

References

1. Takei K, Honda W, Harada S, Arie T and Akita S 2015 Toward Flexible and Wearable Human-Interactive Health-Monitoring Devices. *Advanced Healthcare Materials* **4** 4 487-500.
2. Xie W, He J, Kang HJ, Tang X, Zhu S, Laver M, Wang S, Copley JRD, Brown CM, Zhang Q and Tritt TM 2010 Identifying the Specific Nanostructures Responsible for the High Thermoelectric Performance of (Bi,Sb)2Te3 Nanocomposites. *Nano Letters* **10** 9 3283-3289.
3. Liu W-S, Zhang Q, Lan Y, Chen S, Yan X, Zhang Q, Wang H, Wang D, Chen G and Ren Z 2011 Thermoelectric Property Studies on Cu-Doped n-type CuxBi2Te2.7Se0.3 Nanocomposites. *Advanced Energy Materials* **1** 4 577-587.
4. Meng J-H, Zhang X-X and Wang X-D 2014 Multi-objective and multi-parameter optimization of a thermoelectric generator module. *Energy* **71** 367-376.
5. Lee H 2013 Optimal design of thermoelectric devices with dimensional analysis. *Applied Energy* **106** 79-88.
6. Dunham MT, Barako MT, LeBlanc S, Asheghi M, Chen B and Goodson KE 2015 Power density optimization for micro thermoelectric generators. *Energy* **93, Part 2** 2006-2017.
7. Pietrzyk K, Soares J, Ohara B and Lee H 2016 Power generation modeling for a wearable thermoelectric energy harvester with practical limitations. *Applied Energy* **183** 218-228.
8. Bahk J-H, Fang H, Yazawa K and Shakouri A 2015 Flexible thermoelectric materials and device optimization for wearable energy harvesting. *Journal of Materials Chemistry C* **3** 40 10362-10374.
9. Suarez F, Nozariasbmarz A, Vashaee D and Ozturk MC 2016 Designing thermoelectric generators for self-powered wearable electronics. *Energy & Environmental Science* **9** 6 2099-2113.
10. Leonov V 2011 Human Machine and Thermoelectric Energy Scavenging for Wearable Devices. *ISRN Renewable Energy* **2011** 11.
11. Webb P 1992 Temperatures of skin, subcutaneous tissue, muscle and core in resting men in cold, comfortable and hot conditions. *European Journal of Applied Physiology and Occupational Physiology* **64** 5 471-476.
12. Pennes HH 1948 Analysis of Tissue and Arterial Blood Temperatures in the Resting Human Forearm. *Journal of Applied Physiology* **1** 2 93-122.
13. Chen MM and Holmes KR 1980 MICROVASCULAR CONTRIBUTIONS IN TISSUE HEAT TRANSFER. *Annals of the New York Academy of Sciences* **335** 1 137-150.
14. Jiji LM, Weinbaum S and Lemons DE 1984 Theory and Experiment for the Effect of Vascular Microstructure on Surface Tissue Heat Transfer—Part II: Model Formulation and Solution. *Journal of Biomechanical Engineering* **106** 4 331-341.
15. Wissler EH 1998 Pennes’ 1948 paper revisited. *Journal of Applied Physiology* **85** 1 35-41.
16. Stolwijk JAJ and Hardy JD 1966 Temperature regulation in man — A theoretical study. *Pflüger's Archiv für die gesamte Physiologie des Menschen und der Tiere* **291** 2 129-162.
17. Smith CE 1991 A transient three-dimensional model of the thermal system. PhD thesis (Kansas State University).
18. Fu M, Weng W, Chen W and Luo N 2016 Review on modeling heat transfer and

thermoregulatory responses in human body. *Journal of Thermal Biology* **62, Part B** 189-200.
19. Fiala D, Lomas KJ and Stohrer M 1999 A computer model of human thermoregulation for a wide range of environmental conditions: the passive system. *Journal of Applied Physiology* **87** 5 1957-1972.
20. Huizenga C, Hui Z and Arens E 2001 A model of human physiology and comfort for assessing complex thermal environments. *Building and Environment* **36** 6 691-699.
21. Foda E, Almesri I, Awbi HB and Sirén K 2011 Models of human thermoregulation and the prediction of local and overall thermal sensations. *Building and Environment* **46** 10 2023-2032.
22. Zhang Y, Chad Webb R, Luo H, Xue Y, Kurniawan J, Cho NH, Krishnan S, Li Y, Huang Y and Rogers JA 2016 Theoretical and Experimental Studies of Epidermal Heat Flux Sensors for Measurements of Core Body Temperature. *Advanced Healthcare Materials* **5** 1 119-127.
23. Hussain AM, Lizardo EB, Torres Sevilla GA, Nassar JM and Hussain MM 2015 Ultrastretchable and Flexible Copper Interconnect-Based Smart Patch for Adaptive Thermotherapy. *Advanced Healthcare Materials* **4** 5 665-673.
24. Tanabe S-i, Kobayashi K, Nakano J, Ozeki Y and Konishi M 2002 Evaluation of thermal comfort using combined multi-node thermoregulation (65MN) and radiation models and computational fluid dynamics (CFD). *Energy and Buildings* **34** 6 637-646.
25. Wilson SB 1989 A tissue heat transfer model for relating dynamic skin temperature changes to physiological parameters. *Physics in Medicine and Biology* **33** 8 496.
26. Salloum M, Ghaddar N and Ghali K 2007 A new transient bioheat model of the human body and its integration to clothing models. *International Journal of Thermal Sciences* **46** 4 371-384.
27. Fanger PO 1970 *Thermal comfort: Analysis and applications in environmental engineering* (Danish Technical Press).
28. Bedford T 1936 *The Warmth Factor in Comfort at Work. A Physiological Study of Heating and Ventilation* (London: H.M.S.O.) p iv+102 pp.
29. de Dear RJ, Arens EA, Zhang HPD and Oguro M 1996 Convective and radiative heat transfer coefficients for individual human body segments.
30. Wang X-L 1990 Convective heat losses from segments of the human body. *Climate Buildings* **3** 8-14.
31. Wang X 1990 Convective heat transfer coefficients from head and arms. *Climate Buildings* **2** 3-7.
32. Wang X-L 1990 Free convective heat transfer coefficients of a heated full-scale manikin. *Climate Buildings* **1** 17-31.
33. Yang Y and Liu J 2010 Evaluation of the power-generation capacity of wearable thermoelectric power generator. *Frontiers of Energy and Power Engineering in China* **4** 3 346-357.
34. Chitrphiromsri P and Kuznetsov A 2005 Modeling heat and moisture transport in firefighter protective clothing during flash fire exposure. *Heat and Mass Transfer* **41** 3 206-215.
35. Fiala D 1998 Dynamic Simulation of Human Heat Transfer and Thermal Comfort. Phd thesis (De Montfort University).
36. Chato JC 1980 Heat transfer to blood vessels. *Journal of Biomechanical Engineering* **102** 2 110-118.
37. Munir A, Takada S and Matsushita T 2009 Re-evaluation of Stolwijk's 25-node human thermal model under thermal-transient conditions: Prediction of skin

temperature in low-activity conditions. *Building and Environment* **44** 9 1777-1787.

38. Goldsmid HJ 2010 Theory of Thermoelectric Refrigeration and Generation. *Introduction to Thermoelectricity*, (Springer Berlin Heidelberg, Berlin, Heidelberg), pp 7-21.
39. Yazawa K and Shakouri A 2012 Optimization of power and efficiency of thermoelectric devices with asymmetric thermal contacts. *Journal of Applied Physics* **111** 2 024509.
40. Apertet Y, Ouerdane H, Goupil C and Lecoeur P 2014 Comment on "Effective thermal conductivity in thermoelectric materials" [J. Appl. Phys. 113, 204904 (2013)]. *Journal of Applied Physics* **115** 12 126101.
41. Baranowski LL, Snyder GJ and Toberer ES 2013 Effective thermal conductivity in thermoelectric materials. *Journal of Applied Physics* **113** 20 204904.
42. Smith P and Twizell EH 1984 A transient model of thermoregulation in a clothed human. *Applied Mathematical Modelling* **8** 3 211-216.

Figure Captions

Figure 1. Model diagram of human thermoregulatory system of active and passive systems. Illustration of specific tissue layers near the volar forearm, and simulation model with physiological data on the volar forearm are also provided.

Figure 2. Comparison of the current model with other simulation results and experimental data: (a) experimental test conditions used for model verification: temperature and relative humidity (RH) with time in minutes (mins) of the experiment; (b) variation in skin temperature of the simulation results compared with those based on the Fiala and the Smith human thermoregulatory models[19, 42] and experimentally obtained maximum and minimum average skin temperature values by Munir *et al*.[37] for forehead; (c) and for forearm. Values used for simulation are available in Table 1.

Figure 3. Variation in skin (a) heat flux, (b) temperature, and (c) thermal resistance with respect to changes in ambient temperature and heat transfer coefficient. Values used for simulation are available in Table 1.

Figure 4. (a) Cross sectional view of thermoelectric unit couple. Unit couple consist of *p* and *n* type thermoelectric materials, filler materials, electrodes and heat sink as indicated. (b) Thermal resistance network for the thermoelectric device. Here T_{core} indicates core body temperature, $R_{t,skin}$ indicates skin thermal resistance, $R_{t,contanct}$ indicates skin and device contact thermal resistance, $R_{t,C}$ indicates heat sink thermal resistance ,$R_{t,fill}$ indicates gap

filler thermal resistance, $R_{t,TEG}$ indicates thermoelectric material thermal resistance, $T_{TEG,H}$ indicates hot side thermoelectric element temperature, $T_{TEG,c}$ indicates cold side thermoelectric element temperature and T_a indicates ambient temperature.

Figure 5. (a) Temperature drop across the thermoelectric element versus fill factor calculated based on the variable-skin-thermal-resistance model (VRM) and the constant-skin-thermal-resistance models (CRM), *i.e.*, 0.0135, 0.02, and 0.0666 m^2 K/W. Inset shows electrical conductance versus fill factor calculated based on the models indicating that electrical conductance is independent of the models used. (b) Power output of the CRM and the VRM versus fill factor. Values are from Table 2.

Figure 6. (a) Power output versus heat transfer coefficient calculated based on the variable-skin-thermal-resistance model (VRM) and the constant-skin-thermal-resistance models (CRM), *i.e.*, 0.0135, 0.2, and 0.0666 m^2 K/W. (b) Deviation in power output between the CRM and the VRM under different heat transfer coefficients of the heat sink. Values used in the simulation are available in Table 2.

Figure 7. (a) Refrigerated temperature drop of the skin versus heat transfer coefficient calculated based on the variable-skin-thermal-resistance model (VRM) and the constant-skin-thermal-resistance models (CRM), *i.e.*, 0.0135, 0.02, and 0.0666 m^2 K/W. (b) Heat flux extracted from the skin by the thermoelectric refrigeration versus heat transfer coefficient for the VRM and the CRM. Values used in the simulation are available in Table 2.

Figure 8. Comparison of refrigeration performance between the variable-skin-thermal-resistance model (VRM) and the constant-skin-thermal-resistance models (CRM): (a) temperature drop of the skin and heat flux extracted versus supplied current to the device and (b) power consumption of the device. Initially both models have thermal resistance of 0.021 m^2 K/W. Therefore, the initial skin temperatures of both models are the same. Values used in the simulation are available in Table 2.

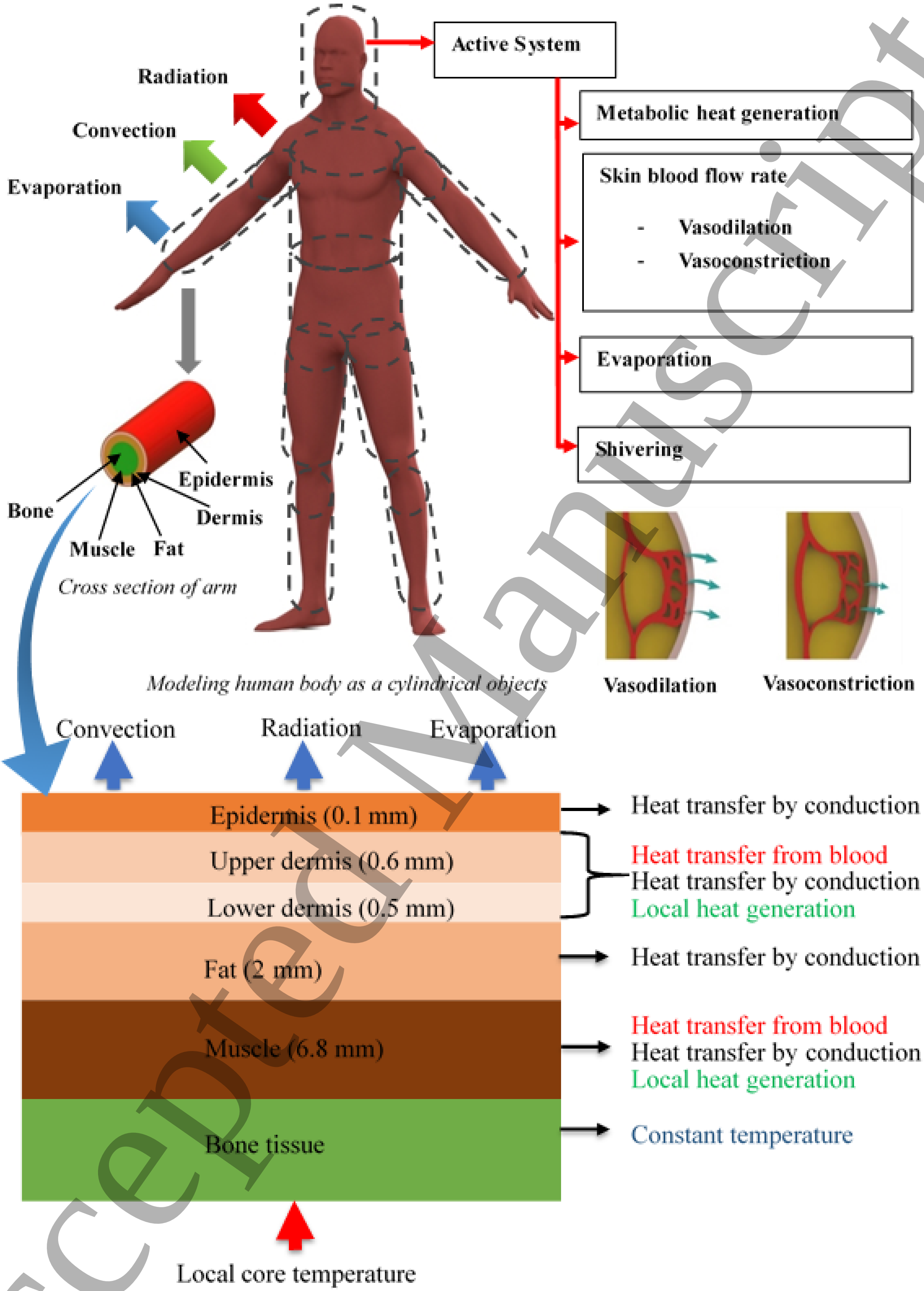
Active System
Metabolic heat generation
Skin blood flow rate
- Vasodilation
- Vasoconstriction
Evaporation
Shivering
Radiation
Convection
Evaporation
Epidermis
Dermis
Bone
Muscle
Fat
Cross section of arm
Modeling human body as a cylindrical objects
Vasodilation
Vasoconstriction
Convection
Radiation
Evaporation
Epidermis (0.1 mm)
Upper dermis (0.6 mm)
Lower dermis (0.5 mm)
Fat (2 mm)
Muscle (6.8 mm)
Bone tissue
Heat transfer by conduction
Heat transfer from blood
Heat transfer by conduction
Local heat generation
Heat transfer by conduction
Heat transfer from blood
Heat transfer by conduction
Local heat generation
Constant temperature
Local core temperature

Figure 1

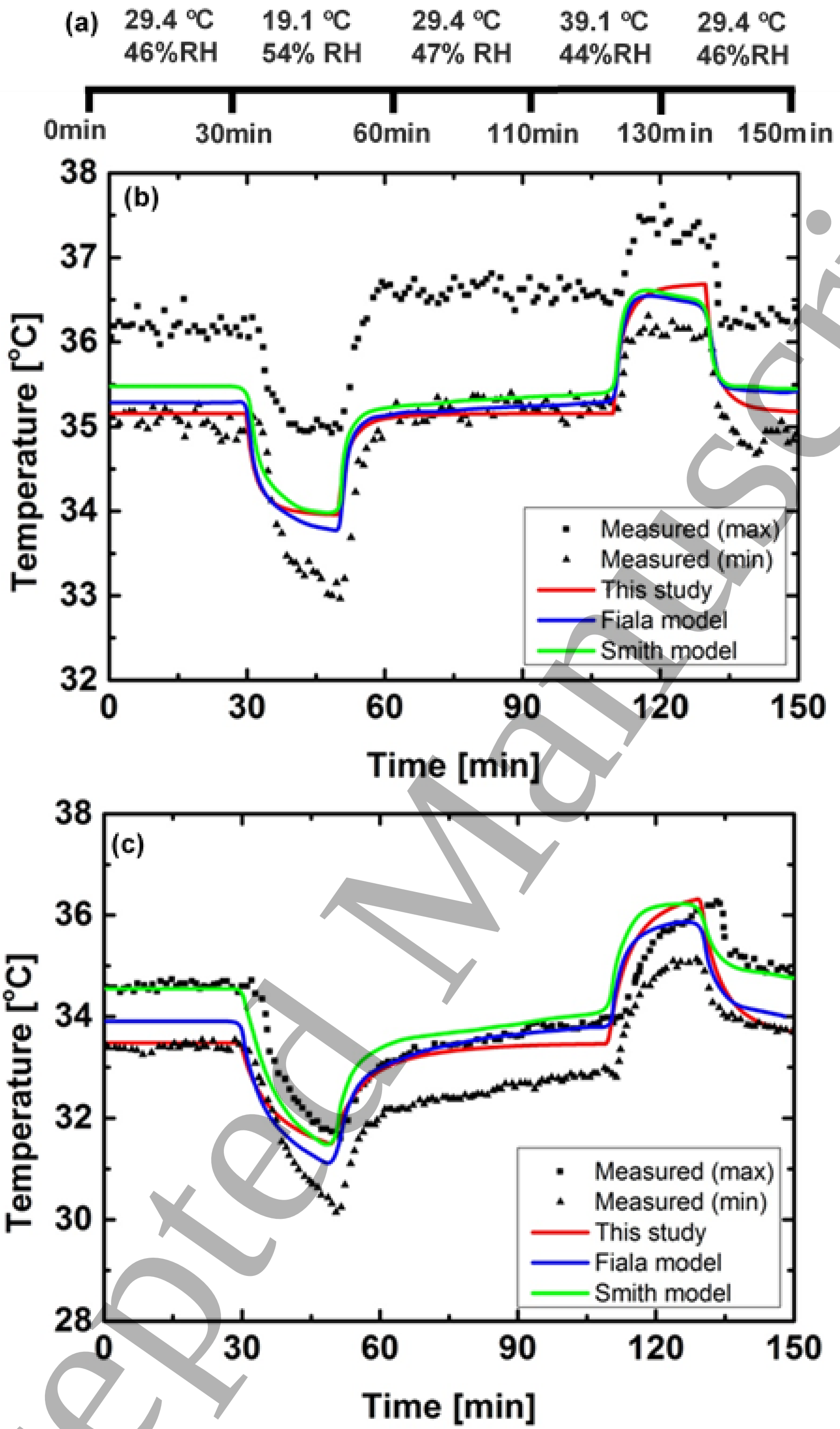
(a)
29.4 °C 46%RH
19.1 °C 54% RH
29.4 °C 47% RH
39.1 °C 44%RH
29.4 °C 46%RH
0min
30min
60min
110min
130min
150min
(b)
Temperature [°C]
Time [min]
Measured (max)
Measured (min)
This study
Fiala model
Smith model
(c)
Temperature [°C]
Time [min]
Measured (max)
Measured (min)
This study
Fiala model
Smith model

Figure 2

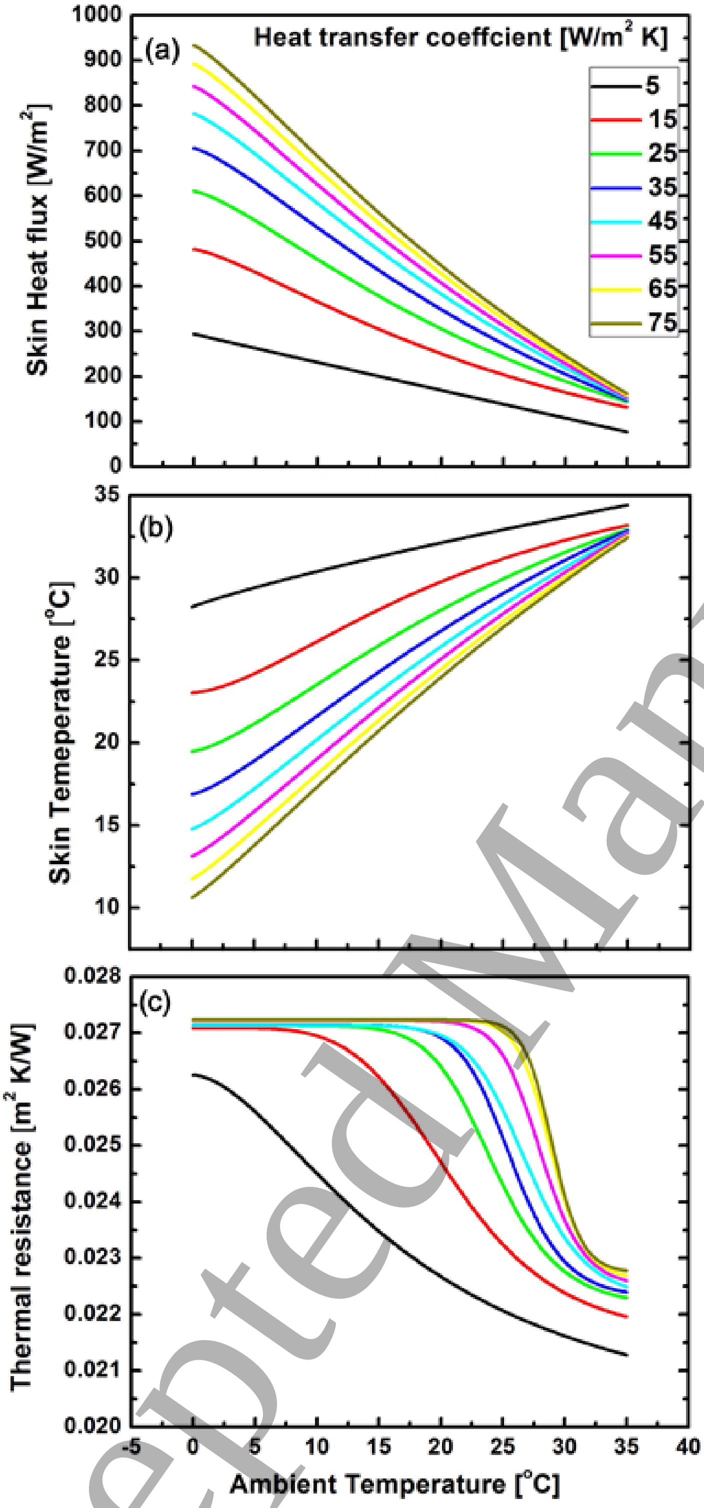
(a)
Heat transfer coeffcient [W/m² K]
5
15
25
35
45
55
65
75
Skin Heat flux [W/m²]
(b)
Skin Temeperature [°C]
(c)
Thermal resistance [m² K/W]
Ambient Temperature [°C]

Figure 3

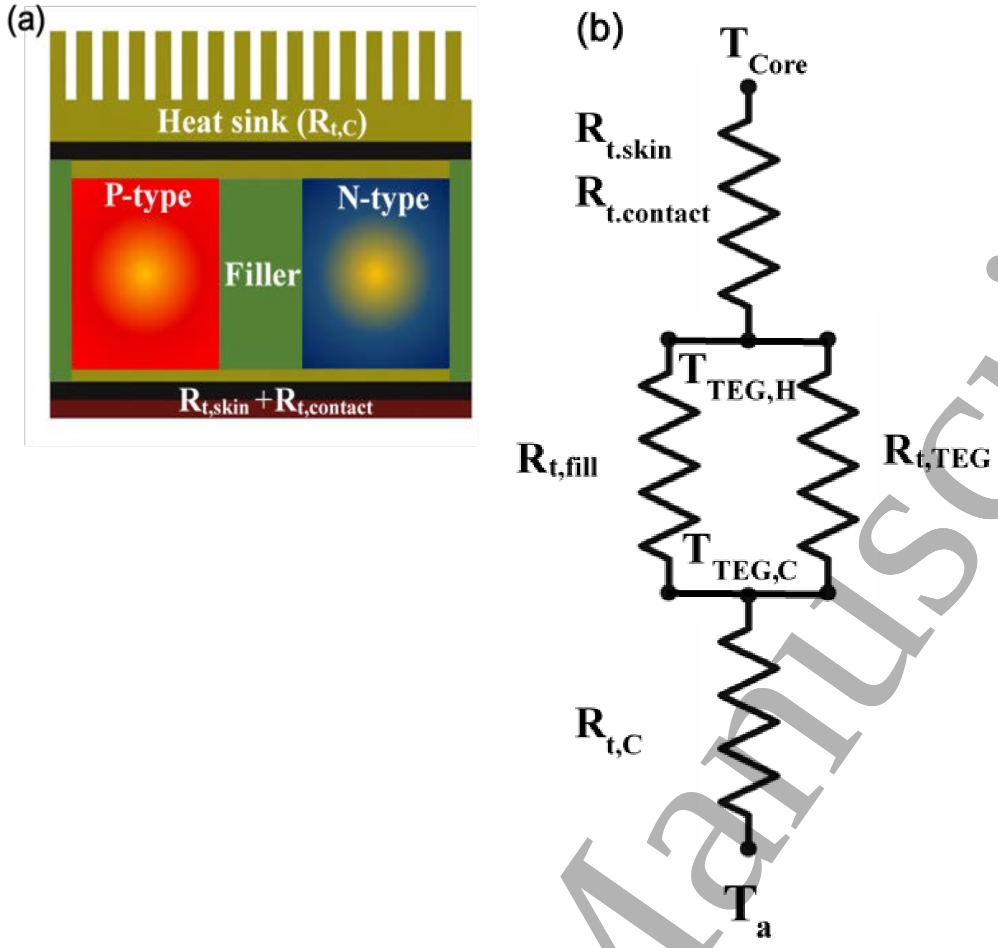
(a)
Heat sink ($R_{t,C}$)
P-type
Filler
N-type
$R_{t,skin}+R_{t,contact}$
(b)
T_{Core}
$R_{t.skin}$
$R_{t.contact}$
$T_{TEG,H}$
$R_{t,fill}$
$R_{t,TEG}$
$T_{TEG,C}$
$R_{t,C}$
T_a

Figure 4

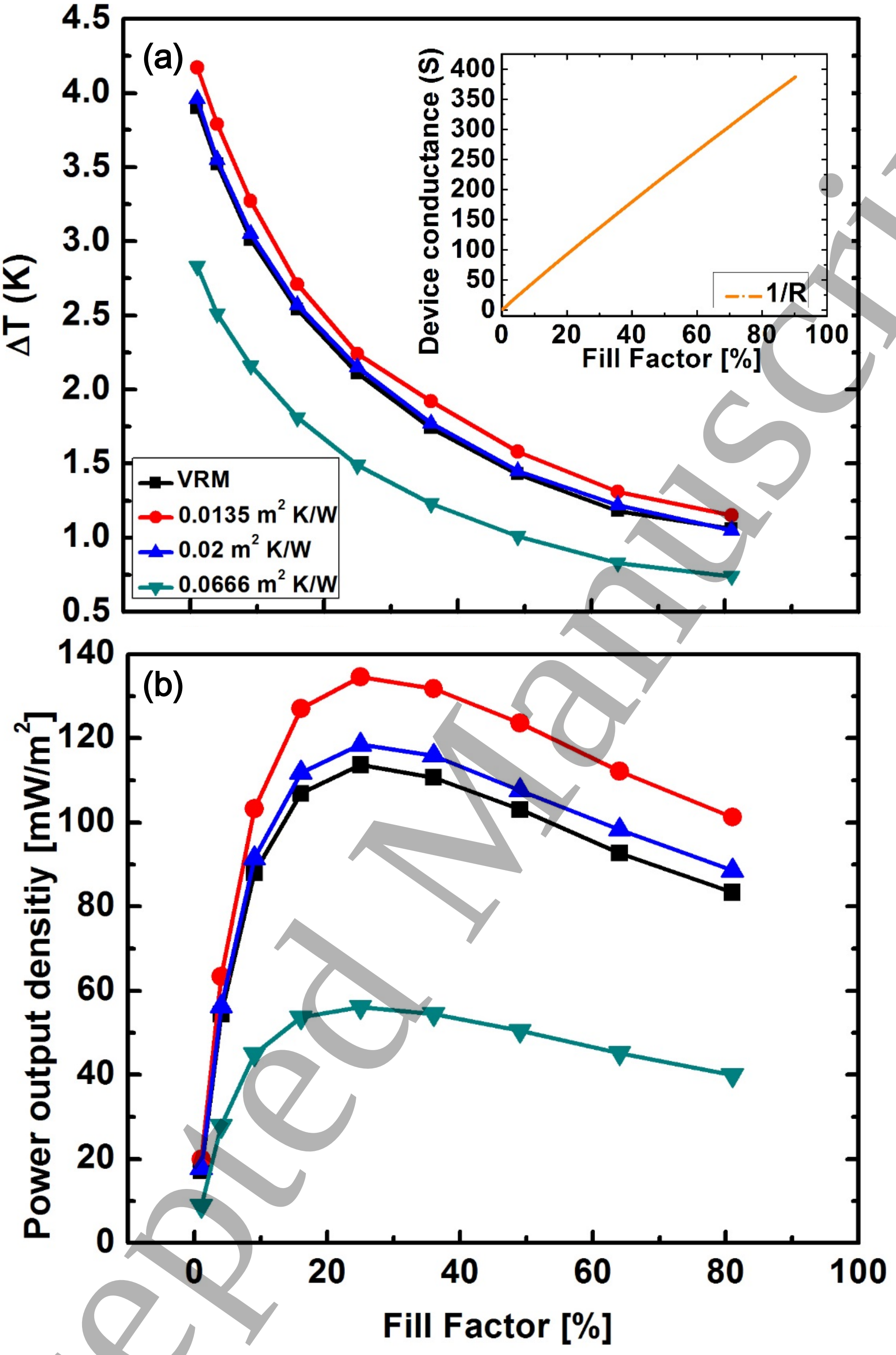
(a)
ΔT (K)
VRM
0.0135 m² K/W
0.02 m² K/W
0.0666 m² K/W
Device conductance (S)
Fill Factor [%]
1/R
(b)
Power output densitiy [mW/m²]
Fill Factor [%]

Figure 5

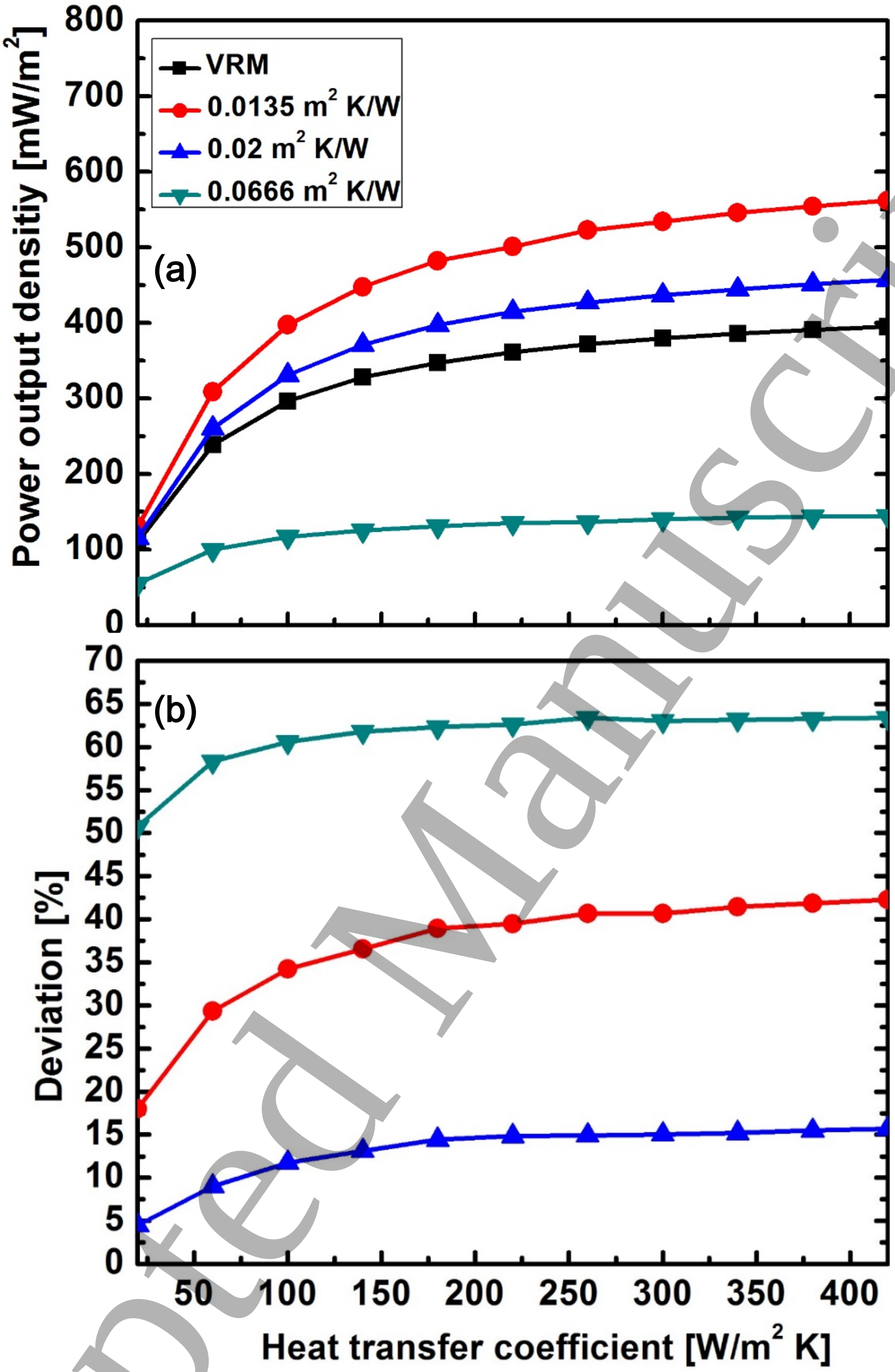
VRM
0.0135 m^2 K/W
0.02 m^2 K/W
0.0666 m^2 K/W
(a)
(b)
Power output densitiy [mW/m^2]
Deviation [%]
Heat transfer coefficient [W/m^2 K]

Figure 6

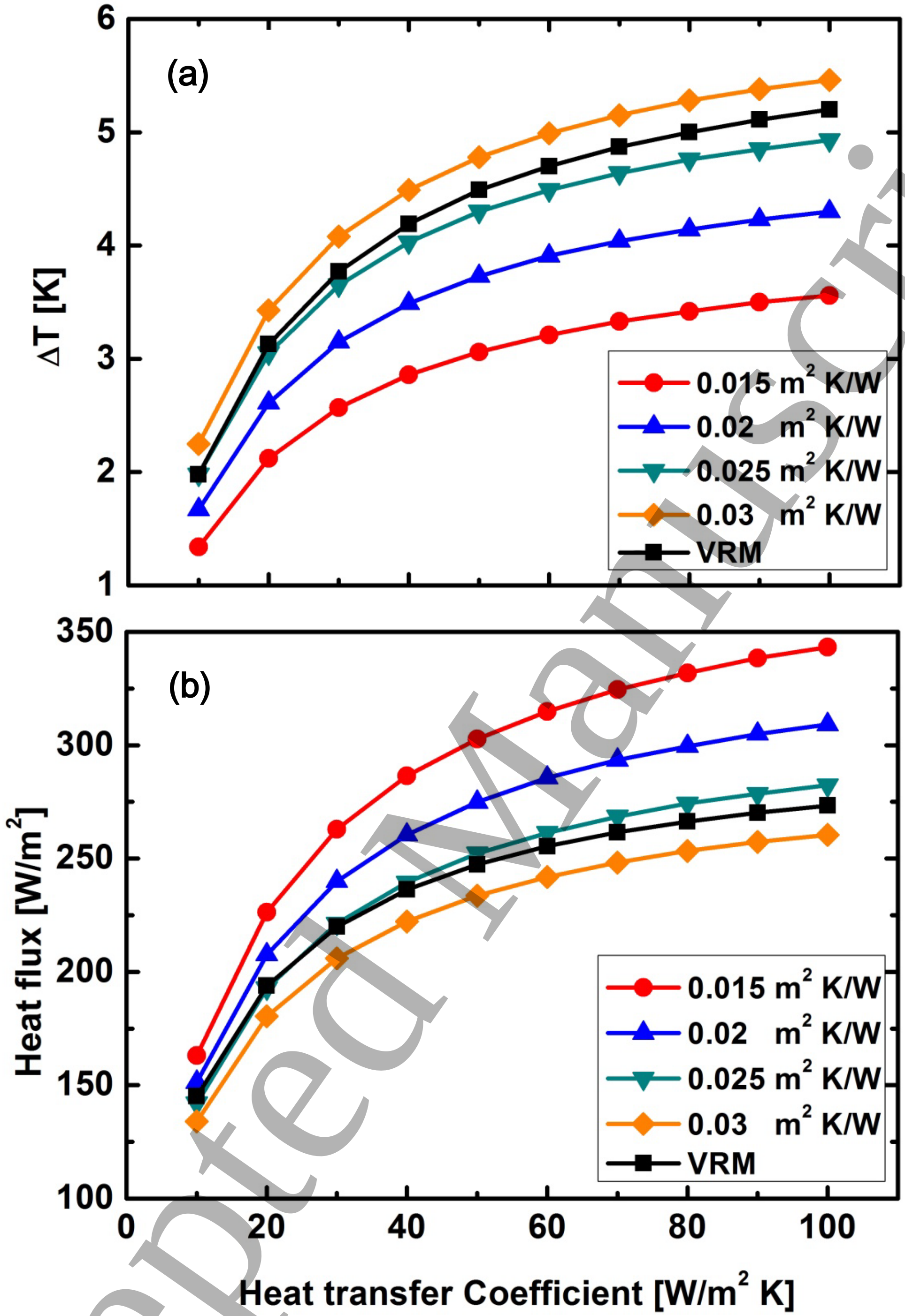
(a)
ΔT [K]
0.015 m² K/W
0.02 m² K/W
0.025 m² K/W
0.03 m² K/W
VRM
(b)
Heat flux [W/m²]
0.015 m² K/W
0.02 m² K/W
0.025 m² K/W
0.03 m² K/W
VRM
Heat transfer Coefficient [W/m² K]

Figure 7

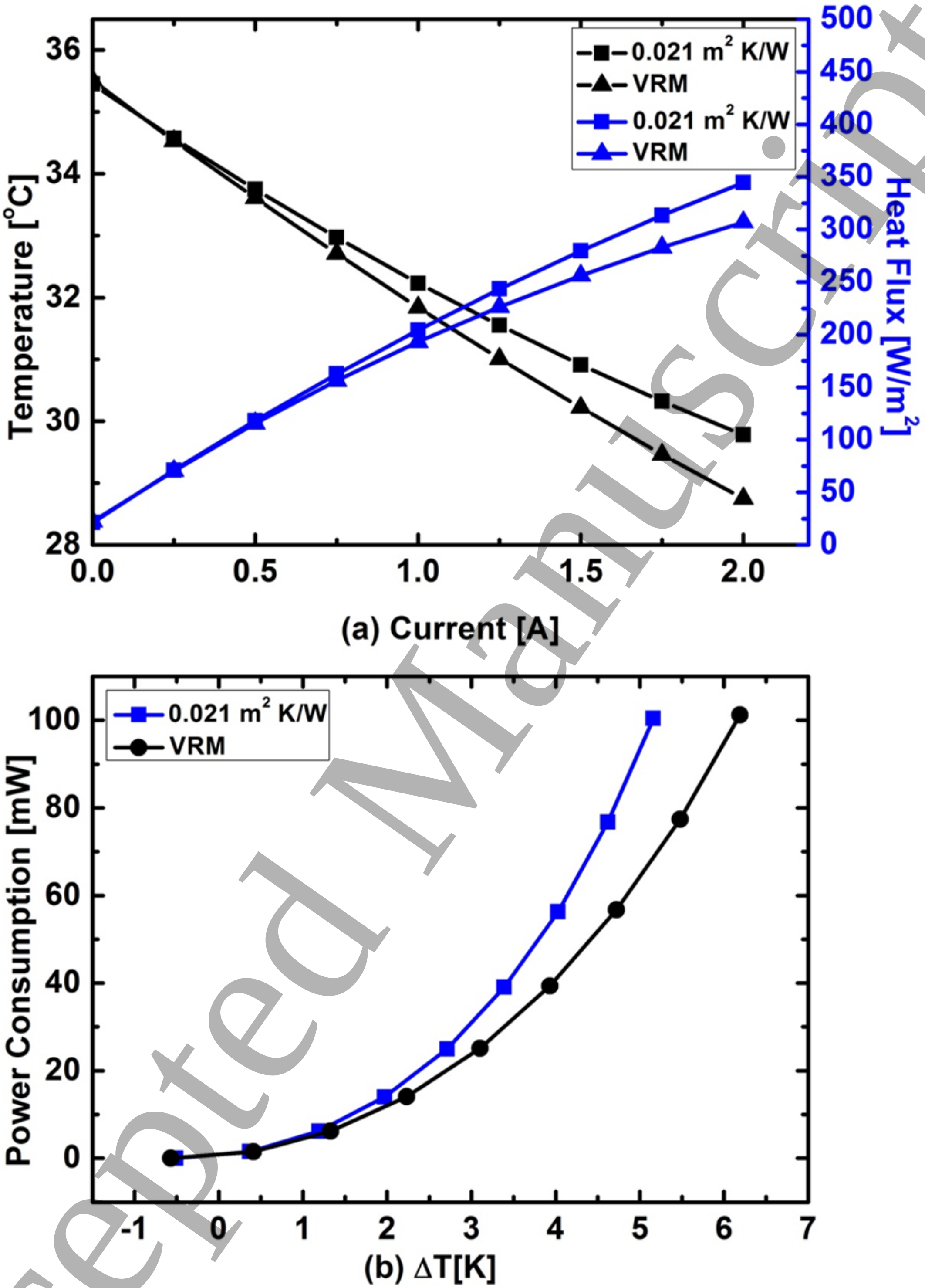
0.021 m² K/W
VRM
0.021 m² K/W
VRM
Temperature [°C]
Heat Flux [W/m²]
(a) Current [A]
0.021 m² K/W
VRM
Power Consumption [mW]
(b) ΔT[K]

Figure 8